Showcasing research from Professor Yoonsoo Pang's laboratory, Department of Chemistry, Gwangju Institute of Science and Technology, Gwangju, Republic of Korea.

Metal-enhanced fluorescence of dyes with quadrupole surface plasmon resonance of silver nanoparticles

The fluorescence of chromophores increases strongly by the localized surface plasmons of metal nanoparticles. Both dipole and quadrupole surface plasmon resonances enhance the fluorescence of dyes located near the metal nanoparticles. This work investigates the detailed mechanisms of fluorescence enhancements with the silver colloidal nanosurfaces composed of homogeneous nanoparticles of 60–220 nm in diameter by time-resolved fluorescence measurements and finite-difference time-domain simulations.

As featured in:

See Yoonsoo Pang *et al.*, *Nanoscale Adv.*, 2022, **4**, 2794.

ROYAL SOCIETY OF CHEMISTRY

rsc.li/nanoscale-advances

PAPER

Check for updates

Metal-enhanced fluorescence of dyes with quadrupole surface plasmon resonance of silver nanoparticles†

Daedu Lee, Junghyun Song, Gyounghyun Song and Yoonsoo Pang ⓘ *

Silver colloidal films (SCFs) composed of homogeneous 60–220 nm silver nanoparticles were synthesized for optimal fluorescence enhancement of chromophores with the dipole and quadrupole surface plasmons. The fluorescence enhancements with the SCFs of three chromophores, 4-(dicyanomethylene)-2-methyl-6-(4-dimethylaminostyryl)-4*H*-pyran, 4-dimethylamino-4′-nitrobiphenyl, and coumarin 343 whose emission spectra are centered distinctively in the 470–560 nm wavelength range were compared. Fluorescence enhancements and lifetime changes were investigated *via* time-resolved fluorescence spectroscopy. The spectral overlap between the chromophore's emission and the dipole or quadrupole surface plasmon resonance (SPR) bands determined the fluorescence enhancements with the SCFs. The dipole and quadrupole SPR bands both appeared to provide effective fluorescence enhancements of chromophores. This knowledge allows researchers to develop sensitive fluorescence sensors by combining nanoparticles with optimal dipole or quadrupole SPR bands in order to achieve fluorescence enhancement of a specific chromophore. The emission dynamics measurements with the SCFs were combined with the finite-difference time-domain simulation results for the local electric fields around the silver nanoparticles to enable discussion of metal-enhanced fluorescence mechanisms, including excitation and emission enhancements.

Introduction

Metal-enhanced fluorescence (MEF) has attracted significant attention as an emerging fluorescence-based technology for biomedical imaging, chemical sensing, organic optoelectronic devices, *etc.*, due to improvements in dye brightness and photostability.[1–7] The locally enlarged electric field around each metal nanoparticle increases the absorption and emission rates of the chromophores. Plasmon-coupled emission also amplifies the chromophores' emission rates.[1,2,8,9] The increase in the local electric field around the metal nanoparticles depends heavily on resonance excitation of the surface plasmon resonance (SPR) band of the metal nanoparticles.[10–12] Plasmon-coupled emissions from the metal nanoparticles are often evidenced by the increased quantum yields and decreased fluorescence lifetimes of the chromophores, which depend on through-space energy transfer between the chromophore's excited states and the SPR bands.[1–3,8,9] The spectral overlap between the SPR bands of the

metal nanoparticles and the chromophore's emission spectrum appears to be critical to achieving strong plasmon-coupled emission.[13–19]

The resonant excitation, the spectral overlap between the fluorophore's emission and the SPR bands of the metal nanoparticles, and the chromophore–nanoparticle distance are among the crucial factors that affect emission enhancement optimization in many MEF applications.[1–3] Fluorescence enhancement by the local electric field of a metal nanoparticle is inversely proportional to the metal-fluorophore distance because the field strength decreases as one moves away from the nanoparticle surface.[9,13,20,21] Plasmon-coupled emissions also increase as the metal-fluorophore distance decreases due to Förster-type resonance energy transfer.[22,23] However, fluorescence quenching, which occurs *via* additional non-radiative decay channels of metal nanoparticle, increases when the chromophores are located within about 10 nm of the nanoparticle surface.[21,24–26] Therefore, efficient fluorescence enhancements are often observed at a metal-fluorophore separation of 10 nm or larger.[21,27–30]

The shape of the surface plasmons or oscillating surface electrons depends strongly on the metal nanoparticle size.[31,32] The surface plasmons of the small nanoparticles (those with diameters that are much smaller than the wavelength of the incident radiation) appear uniformly polarized along the incident electric field. This represents the dipole SPR mode (see

Department of Chemistry, Gwangju Institute of Science and Technology, 123 Cheomdangwagi-ro, Buk-gu, Gwangju 61005, Republic of Korea. E-mail: ypang@gist.ac.kr

† Electronic supplementary information (ESI) available: Extinction spectra of silver colloidal nanoparticles; film thickness measurements; FDTD simulation results; emission kinetics of DCM, DNBP, and C343 with the SCFs. See https://doi.org/10.1039/d1na00837d

Fig. S1†). For large nanoparticles (those with a diameter comparable to the wavelength of incident radiation) the surface plasmons are polarized inhomogeneously throughout the nanoparticles with some phase retardation. This represents the multipole (quadrupole) SPR modes appearing as new bands in shorter wavelengths (see Fig. S1†). The phase retardation in larger nanoparticles induces the red-shifts and band broadening of the dipole SPR bands in addition to the appearance of the multipole SPR modes.[31,33,34] Strong quadrupole SPR bands are often observed in the visible wavelengths from anisotropic metal nanoparticles such as silver triangular plates and cubes,[35–39] as well as larger gold or silver colloidal nanoparticles.[34,40,41] The spectral shifts of quadrupole SPR bands originate from changes in the particle diameter, the edge length, or the curvature radius of an anisotropic nanoparticle.[34–41]

Fluorescence enhancements of dyes with the dipole SPR bands of metal nanoparticles have been reported numerously for a wide range of applications. However, only a few studies have reported enhancements with the quadrupole SPR bands.[38] Zhou and co-workers showed that the quadrupole SPR modes of silver nanoplates produce larger resorufin fluorescence enhancements than the dipole SPR modes.[38] Halas and co-workers reported MEF of indocyanine green dye with the dipole and quadrupole SPR bands of gold–silica nanoshells, where increases in radiative decay rates were evaluated only for the dipole SPR modes.[14] Although fluorescence enhancements by the quadrupole SPR modes of silver and gold nanoparticles were demonstrated in these studies, detailed analyses of the fluorescence enhancements based on time-resolved fluorescence measurements have not been used to compare dipole and quadrupole SPR bands. In addition, plasmon-coupled emission accompanying energy transfer between the quadrupole SPR modes and the dyes' excited states has not been reported yet.

We recently reported MEF of 4-(dicyanomethylene)-2-methyl-6-(4-dimethylaminostyryl)-4H-pyran (DCM) and rhodamine 700 with silver colloidal films (SCFs) prepared from highly homogeneous silver colloidal nanoparticles.[17] Although the dipole and quadrupole SPR bands of the SCFs in the visible and near-infrared wavelengths exhibited strong dependence on the particle diameter (67–193 nm), fluorescence enhancement of the dyes has only been observed with the dipole SPR bands of the SCFs via time-resolved fluorescence measurements. The fluorescence enhancements induced by the locally enlarged electric field around the silver nanoparticles were estimated using finite-difference time-domain (FDTD) simulations. The contribution of the plasmon-coupled emission to the total fluorescence enhancement was estimated based on the experimental data for the quantum yield and emission kinetics of dyes with SCFs.

In this study, we extended our research to understanding the detailed mechanisms of MEF by the quadrupole SPR modes of SCFs. The fluorescence enhancements of several dyes that emit in the blue-green region of the visible spectrum, including DCM, 4-dimethylamino-4′-nitrobiphenyl (DNBP), and coumarin 343 (C343), were explored with both the dipole and quadrupole SPR bands of SCFs. Time-resolved fluorescence measurements and FDTD simulations of the local electric field around the SCFs were combined to explain the SCF-induced fluorescence enhancements and the emission kinetics changes.

Experimental

Preparation and characterization of homogeneous SCFs

Silver nitrate (Daejung Chemicals and Metals, Siheung, Korea); C343 and DCM (Sigma-Aldrich, St Louis, MO, USA); DNBP (Tokyo Chemical Industry, Tokyo, Japan); and all other chemicals were used as received without further purification. Homogeneous silver colloidal nanoparticles with diameters of 59–219 nm were synthesized via a kinetically controlled seeded-growth method.[40] The SCFs were prepared by attaching the silver nanoparticles to glass slides that were pre-coated with poly(diallyldimethylammonium chloride).[17] Half of the SCFs were removed using a dilute nitric acid solution for the evaluation of the fluorescence enhancement. Then, 1.0% (w/v) polystyrene (PS; avg. m.w. 208 000; Wako Pure Chemical, Osaka, Japan) solutions in tetrahydrofuran (Samchun Chemicals, Seoul, Korea) containing fluorophores (C343, DCM, or DNBP in the concentration of 2×10^{-4} M) were spin-coated on the SCFs. The thicknesses of the spin-coated PS films were determined as 180 nm from the interference patterns in the UV-vis absorption spectrum (see Fig. S2†).[42,43] The steady-state extinction spectra of the SCFs were measured using a Mega-900 UV-vis spectrophotometer (Scinco, Seoul, Korea), and scanning electron microscope (SEM) images of the SCFs were obtained using a JSM-7500F field emission SEM (Jeol, Tokyo, Japan).

Steady-state and time-resolved fluorescence measurements

A time-correlated single-photon counting setup with a PicoHarp 300 (PicoQuant, Berlin, Germany) and a picosecond diode laser (P-C-405; PicoQuant) was used for the steady-state and time-resolved fluorescence measurements.[17,19,44] Excitation pulses at 405 nm (approximately 4 pJ per pulse at a 10 MHz repetition rate) were focused at a sample with a diameter of about 150 μm. An instrument response function (IRF) of approximately 150 ps (full width half maximum) was obtained.[19] All of the fluorescence spectra and kinetics were averaged over 15 random positions on each SCF to minimize any local SCF effects.

Finite-difference time-domain simulations

The local electric field distribution around the silver nanoparticles of each SCF was estimated using FDTD simulations by the commercial software Lumerical (Lumerical Inc., Vancouver, Canada). Nanospheres with a specific diameter between 59 and 219 nm were placed in the center of a 1500 nm-long simulation cube, and the boundary condition of the perfectly matched layer was used. The dielectric constant of silver,[45] the refractive index of the PS medium ($n = 1.581$), and a simulation time of 500 fs were used with 405 nm excitation. In addition, a mesh override region with a volume of (particle diameter + 200)^3 nm^3 and a mesh size of 1.0 nm was used to provide more accurate simulations. The local electric field exhibited only minor dependence on the mesh size (within 0.5–1.0 nm range) in the

mesh convergence test shown in Fig. S3.† This validates the choice of a 1.0 nm mesh for the FDTD simulations. The local electric field distributions were evaluated on a two-dimensional plane that included the electric field and the wave vectors of the incident electromagnetic radiation.

Results and discussion

Dipole and quadrupole SPR bands of SCFs

Fig. 1 shows SEM images and particle diameter distributions of SCFs prepared with homogeneous silver nanoparticles.[17,40] The average particle diameters of SCF1–SCF8 (labeled by increasing average particle diameter) are estimated based on the SEM images as 59 ± 6, 66 ± 7, 93 ± 9, 116 ± 11, 129 ± 12, 153 ± 16, 188 ± 17, and 219 ± 22 nm, respectively. It appears that all of the SCFs consist of homogeneous silver nanoparticles grown selectively *via* the seeded-growth method. Particle aggregates that lead to inhomogeneous broadening of the SPR bands are absent from all of the SCFs.

The extinction spectra of SCFs within thin PS layers are compared in Fig. 2(a). The extinction spectra of SCFs composed of small silver nanoparticles (SCF1–SCF3 with average particle diameters of 59–93 nm) appear mainly as dipole SPR bands at 489–557 nm. The dipole SPR bands exhibit monotonous red-shifts towards 900 nm as the particle diameter increases to 219 nm (SCF8). The dipole SPR bands also exhibit spectral broadening as the average particle diameter of SCFs increases. In the extinction spectra of SCFs composed of large silver nanoparticles (SCF4–SCF8 with average particle diameters of 116–219 nm), additional SPR bands appear in the 400–550 nm wavelength range. These additional bands that appear at

Fig. 2 (a) Extinction spectra and (b) dipole (red circles) and quadrupole (blue squares) SPR wavelengths for SCF1–SCF8 within thin PS layers as a function of the particle diameter. The SPR wavelengths of the corresponding silver nanoparticles used in the synthesis of each SCF, which were obtained in aqueous solution, are indicated using dotted lines (red for dipole and blue for quadrupole).
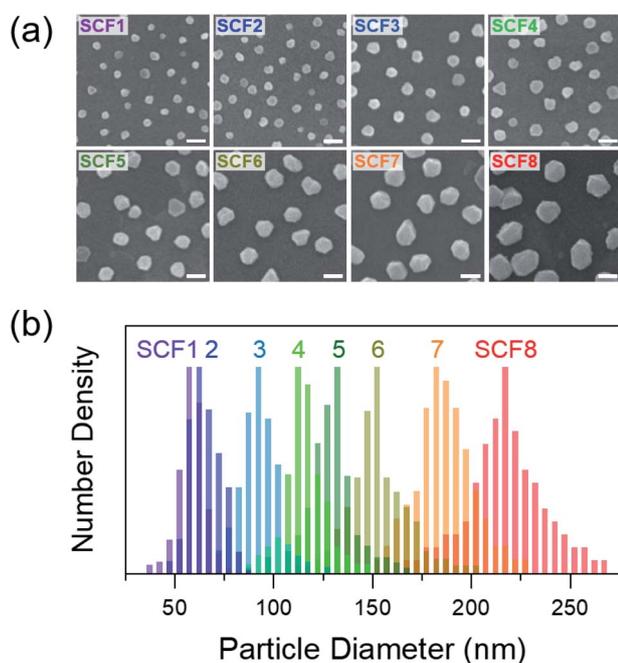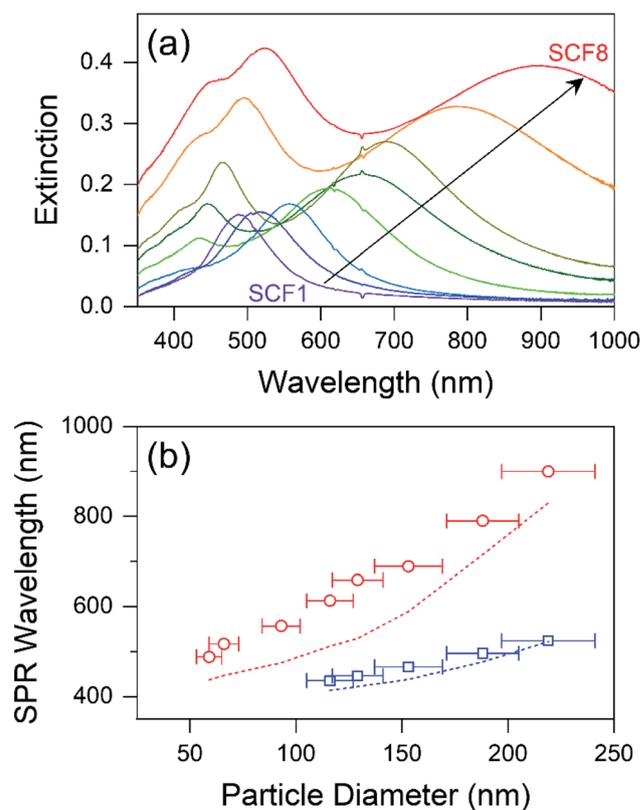

Fig. 1 (a) SEM images and (b) particle size distributions of silver colloidal films (SCFs) labeled SCF1–SCF8 in the order of increasing average particle diameter (59–219 nm). Each scale bar is 200 nm long.

shorter wavelengths than the dipole SPR band of each SCF are multipole SPR bands. The strongest multipole SPR bands are the quadrupole SPR bands, which exhibit similar red-shifts from 435 nm (SCF4) to 523 nm (SCF8) as the average particle diameter increases. Fig. S4† compares the surface charge density distributions of the silver nanoparticles in SCF5 and SCF8 determined from FDTD simulations. The results support assignment of the extinction bands in the 489–900 nm range as dipole SPR modes and additional bands in the 400–550 nm range as quadrupole SPR modes.

The maximum dipole and quadrupole SPR wavelengths of SCFs are compared to those of the corresponding silver nanoparticles in an aqueous solution in Fig. 2(b). The dipole and quadrupole SPR bands of the silver nanoparticles used for SCF synthesis are quite similar to those reported previously by Bastús *et al.*[34] The dipole and quadrupole SPR bands of the SCFs appear substantially red-shifted from the SPR bands of the corresponding silver nanoparticles in solution: 50–120 nm for the dipole and approximately 20 nm for the quadrupole SPR bands. The red-shifts in the SPR bands of the SCFs from those of corresponding silver nanoparticles in aqueous solution originate from the differences in the refractive indices of the media; $n_{PS} = 1.581$ for PS and $n_{water} = 1.333$ for water.[31,34] Bastús *et al.* reported similar red-shifts in the dipole and quadrupole

SPR bands of silver nanoparticles in the high refractive index medium of polyethylene glycol (PEG; $n_{PEG} = 1.465$), which has also been confirmed *via* Mie theory simulations.[34]

Metal nanosurfaces with homogeneous particle distributions and minimal aggregates can be ideal for MEF studies, where efficient differentiation between the characteristic SPR bands of metal nanoparticles and the absorption and emission bands of fluorophores, and the excitation-dependent fluorescence enhancement analysis are generally required. Numerous gold nanofilms composed of gold nanoparticles with a wide range of particle diameters (20–250 nm) have been reported.[46–48] However, inevitable formation of particle aggregates that result in strong red-shifts and spectral broadening of the SPR bands was reported in these studies. Silver nanosurfaces based on colloidal and island nanoparticles have also been reported for fluorescence enhancements of several chromophores.[49–53] However, small (<100 nm) colloidal nanoparticles are considered inadequate for the MEF study due to the narrow spectral range of the dipole SPR bands. Inhomogeneous island nanoparticles appear problematic due to the spectral broadening of the SPR bands which arises from particle size inhomogeneity.

As shown in Fig. 1 and 2, the SCFs prepared from homogeneous silver nanoparticles in aqueous solution contain well-dispersed monolayer silver substrates with high particle size homogeneity and the absence of particle aggregates, even when large silver nanoparticles up to 220 nm in diameter are used. The dipole and quadrupole SPR bands of the SCFs can be controlled over a wide range of visible and near-infrared wavelengths (400–1000 nm) by using nanoparticles with different average particle diameters. The SCFs reported in this work *via* simple wet synthetic methods are among the optimal substrates for many fluorescence applications, including mechanistic studies of MEF and biological complex fluorophores with high quantum yields.

Fluorescence enhancements of dyes with dipole and quadrupole SPR of SCFs

Fig. 3 shows fluorescence enhancement of the dyes DCM, DNBP, and C343, which are spin-coated in thin PS layers on top of the SCFs. Fluorescence enhancements of the dyes were plotted as a function of the dipole and quadrupole SPR wavelengths of the SCFs, and the absorption and emission spectra of each dye are shown for reference. Dyes with various emission maxima in the 465–555 nm wavelength range are used in this study so that the relevance of the fluorescence enhancements to the spectral overlap between the dyes' emission spectra and the dipole or quadrupole SPR bands of the SCFs can be explored. The emission band of DCM is centered at 555 nm and exhibits the largest spectral overlap with the dipole SPR of SCF3 (at 557 nm) and the quadrupole SPR of SCF8 (at 523 nm).[17,54] Similarly, the emission spectra of DNBP (at 505 nm) and C343 (at 465 nm) exhibit the largest spectral overlaps with the dipole SPR bands of SCF2 (at 517 nm) and SCF1 (at 489 nm), respectively, and with the quadrupole SPR bands of SCF7 (at 496 nm) and SCF6 (at 466 nm), respectively. Fluorescence enhancement of the dyes by the SCFs was evaluated by comparing the average emission
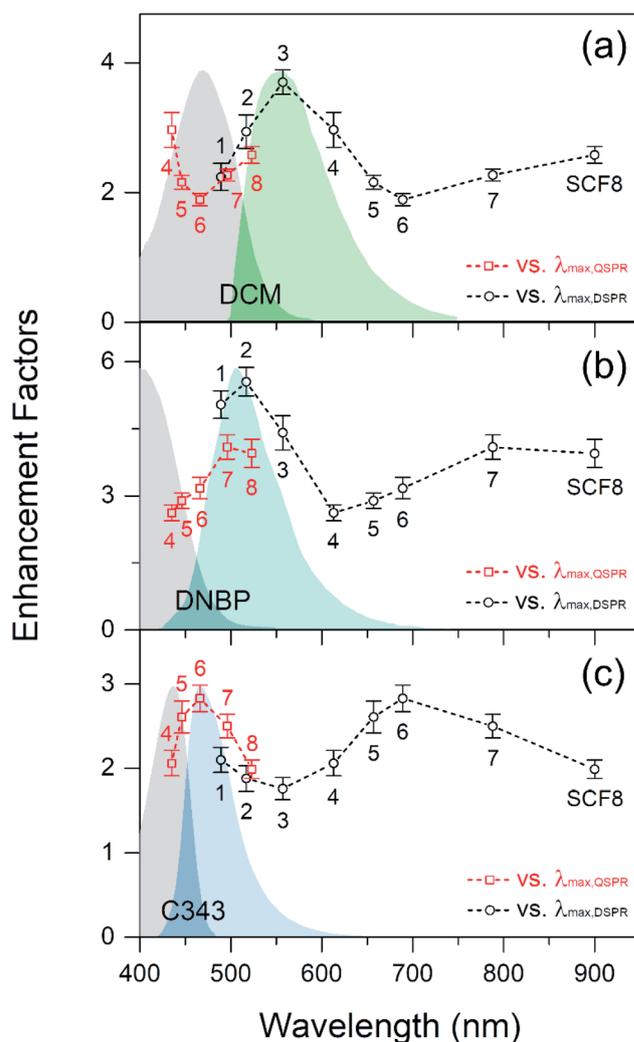

Fig. 3 Fluorescence enhancements of (a) DCM, (b) DNBP, and (c) C343 dispersed in thin PS layers over the SCFs as a function of the dipole (black circles) and quadrupole (red squares) SPR wavelengths. The absorption and emission spectra of each dye are also shown for comparison. The emission spectra are obtained from dyes dispersed in thin PS films using 405 nm excitation. The absorption spectra are observed from dyes dissolved in PS solutions due to low absorbance of dyes in thin PS films.

intensities with and without the SCFs.[17] The emission intensities of DCM at 535–575 nm, DNBP at 485–525 nm, and C343 at 445–485 nm were evaluated for fluorescence enhancement. The geometric factor, f_{geom} represents the ratio of the curved surface area of a PS film with embedded silver nanoparticles to that of a flat, bare film surface. It is evaluated by adding the total hemisphere surface areas of the embedded nanoparticles, A_{hs}, and the bare surface area, A_{bare}, per 1 μm² surface area of the substrate.[17] Details of the fluorescence enhancements of the dyes with SCFs are summarized in Table 1, where the experimentally observed fluorescence enhancements are adjusted further by the geometric factor, f_{geom}.

As shown in Fig. 3(a), the DCM emission increases strongly (3.7 times) with SCF3. The emission band of DCM exhibits the largest spectral overlap with the dipole SPR bands of SCFs. The

Table 1 Fluorescence enhancements of DCM, DNBP, and C343 in PS Films [a]

SCF	$2\bar{R}$ (nm)	$\bar{N}$ (μm^{-2})	A_{hs} (μm^2)	A_{bare} (μm^2)	f_{geom}	Fluorescence enhancements[b]		
						DCM	DNBP	C343
SCF1	59	18	0.10	0.95	1.05	2.2 (2.4)	5.0 (5.3)	2.1 (2.2)
SCF2	66	21	0.14	0.93	1.07	2.9 (3.2)	5.6 (6.0)	1.9 (2.0)
SCF3	93	15	0.20	0.90	1.10	3.7 (4.1)	4.4 (4.9)	1.8 (1.9)
SCF4	116	14	0.30	0.85	1.15	3.0 (3.4)	2.6 (3.0)	2.1 (2.4)
SCF5	129	10	0.26	0.87	1.13	2.2 (2.4)	2.9 (3.3)	2.6 (3.0)
SCF6	153	8	0.29	0.85	1.15	1.9 (2.2)	3.2 (3.6)	2.8 (3.3)
SCF7	188	7	0.39	0.81	1.19	2.3 (2.7)	4.1 (4.9)	2.5 (3.0)
SCF8	219	7	0.53	0.74	1.26	2.6 (3.3)	3.9 (5.0)	2.0 (2.5)

[a] $2\bar{R}$: average diameter; $\bar{N}$: surface number density of particles; $A_{hs} = \bar{N} \times 2\pi\bar{R}^2$: total hemisphere surface area of embedded nanoparticles (per 1 μm^2 surface area); $A_{bare} = 1 - \bar{N} \times \pi\bar{R}^2$: the surface area where no nanoparticle exists (per 1 μm^2 surface area); $f_{geom} = (A_{hs} + A_{bare})/(1\ \mu m^2)$: the geometric factor for the increased surface area. [b] Fluorescence enhancements: the numbers inside the parentheses are observed values. Those outside the parentheses are corrected values for the surface area increase due to embedded nanoparticles.

emission band of DNBP appears at a shorter wavelength than that of DCM. Accordingly, the DNBP emission intensities shown in Fig. 3(b) increase most (5.6 times) when SCF2 is used. SCF2 consists of smaller (66 nm diameter) silver nanoparticles than SCF3 and exhibits substantial spectral overlap with the emission band of DNBP. Thus, the spectral overlap between the dyes' emission bands and the dipole SPR bands of the SCFs appears to be critical to the fluorescence enhancement. This has been observed in many experimental studies.[13–17] The C343 emission band is blue-shifted further (465 nm) from those of DCM and DNBP. It exhibits only partial spectral overlap with SCF1, which is composed of the smallest nanoparticles. The emission of C343 exhibits minor enhancements (up to 2.1 times in the presence of SCF1) with the dipole SPR bands of SCFs. Overall, the dyes' emission intensities exhibit strong dependence on spectral overlap with the dipole SPR bands of the SCFs. With the increase of nanoparticle size, the dipole SPR bands of SCFs are red-shifted away from the emission maximum of each dye. Thus, the emission intensity of each dye exhibits an apparent decrease as the dipole SPR bands of SCFs red-shift: SCF3 → SCF6 for DCM, SCF2 → SCF4 for DNBP, and SCF1 → SCF3 for C343.

Upon increasing the particle size of SCFs further, all of the dyes' emission intensities increase as the spectral overlaps between the emission bands of the dyes and the quadrupole SPR bands of the SCFs become larger. The emission of DCM becomes largest (2.6 times) in the presence of SCF8, where significant spectral overlap with the quadrupole SPR bands of SCFs occurs. Similarly, the emission intensities of DNBP and C343 increase most in the presence of SCF7 (4.1 times) and SCF6 (2.8 times), respectively, where the spectral overlap with the quadrupole SPR bands of SCFs is largest. To summarize the fluorescence enhancements with SCFs, the spectral overlaps between the dyes' emission spectra and both the dipole and quadrupole SPR bands of SCFs lead to emission intensity increases. Dipole SPR bands appear to contribute more to the emission enhancements of DCM and DNBP than quadrupole SPR bands. On the other hand, quadrupole SPR bands appear

more efficient in the emission enhancement of C343 than dipole SPR bands, but this may be due to the partial spectral overlap with SCF1, which contains the smallest nanoparticles. It is interesting to note that the quadrupole SPR bands of SCFs show similar efficiency as the dipole SPR bands with regard to the emission enhancement of dyes located close to the nanoparticles. However, the dyes' emission enhancements induced by the dipole and quadrupole SPR bands of SCFs were not clearly understood yet.

Recently, Zhou and co-workers reported strong fluorescence enhancement of resorufin *via* quadrupole SPR from large silver nanoplates.[38] It is thought that the emission enhancement by silver nanoplates originates mainly from increases in the local electric field caused by the quadrupole SPR. However, the spectral overlaps between the emission spectrum of resorufin and the dipole and quadrupole SPR bands of silver nanoplates also appear to be important to fluorescence enhancement. This is thought to be closely related to plasmon-coupled emissions.[13–17,19,55] Plasmon-coupled emissions are often evidenced by changes in emission kinetics, such as increases in radiative decay rates and decreases in excited state lifetimes. Thus, further details of the dyes' emission enhancements by the dipole and quadrupole SPR bands of SCFs are explored *via* time-resolved fluorescence measurements.

Energy transfer and plasmon-coupled emission with quadrupole SPR of SCFs

Fig. 4 shows the time-resolved fluorescence kinetics of DCM, DNBP, and C343 in thin PS layers on SCFs and bare surfaces, which were excited at 405 nm and probed at 555, 505, and 465 nm, respectively. The fluorescence kinetics of the dyes were fit to a bi-exponential function convoluted with the Gaussian instrument response function (IRF), as shown in Fig. 4. The kinetics of C343 on bare glass was fit to a mono-exponential function convoluted with the Gaussian IRF. The detailed fluorescence kinetics of dyes with and without SCFs, including the intensity-weighted average lifetimes,[56] are summarized in Table S1.†
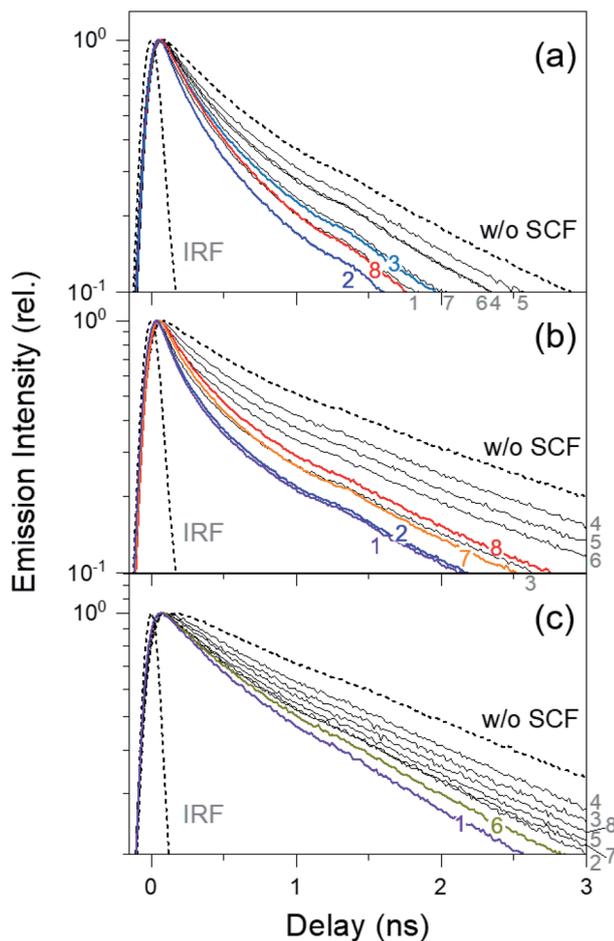
Fig. 4 Time-resolved fluorescence spectra of (a) DCM probed at 555 nm, (b) DNBP probed at 505 nm, and (c) C343 probed at 465 nm. The dyes are dispersed in thin PS films on top of the SCFs. The emission kinetics of dyes without the SCF are also compared. The instrument response function (IRF) represents the time resolution of the fluorescence kinetic measurements. The numbers 1–8, in the matching colors as those of kinetic traces, denote the SCFs (SCF1–SCF8) used for the emission measurements.

As shown in Fig. 4, the fluorescence lifetime of DCM in a thin PS film (1.49 ns without SCF) is shortest (0.88 ns) when SCF2 is present. Upon increasing the silver nanoparticle diameter from 66 nm (SCF2) to 129 nm (SCF5), the DCM lifetime increases to 1.26 ns. The lifetimes of DNBP (2.12 ns without SCF) and C343 (2.54 ns without SCF) are shortest in the presence of SCF1 (1.21 ns for DNBP, 1.82 ns for C343). Similarly, the lifetimes of both dyes increase to 1.88 ns (DNBP) and 2.47 ns (C343) when the nanoparticle diameter increases from 59 nm (SCF1) to 116 nm (SCF4). Further increasing the silver nanoparticle size decreases the fluorescence lifetime of DCM to 0.93 ns (SCF8). The lifetime of DNBP decreases to 1.33 ns (SCF7) and increases slightly to 1.41 ns (SCF8) when the nanoparticle size increases. Similarly, the lifetime of C343 decreases to 1.97 ns (SCF6) and increases again to 2.27 ns (SCF8) when the nanoparticle size increases. The lifetimes of these dyes in the presence of SCFs appear strongly correlated with the fluorescence enhancements shown

in Fig. 3, which also depend heavily on spectral overlap between the dipole or quadrupole SPR bands of the SCFs and the emission bands of dyes. For example, the lifetime of DCM mostly decreases with SCF2 and SCF3, which is interpreted as the increased spectral overlap between the dipole SPR bands and the emission spectrum of DCM. The emission lifetime of DCM decreases with SCF8 as well, which is related to the spectral overlap between the quadrupole SPR band and the emission spectrum. The strong correlation between the fluorescence enhancements and lifetime reductions indicates that MEF with SCFs may be attributed to plasmon-coupled emission that accompanies energy transfer between excited dyes and the dipole or quadrupole SPR modes of the SCFs.

Nevertheless, the fluorescence enhancements and lifetime decreases, which depend on the spectral overlap between the dyes' emission spectra and the dipole and quadrupole SPR bands of the SCFs, appear slightly different from each other. For example, the emission lifetime of DCM with SCF3 (1.03 ns) is longer than those with SCF1 (0.99 ns) or SCF2 (0.88 ns). However, the dipole SPR band of SCF3 exhibits the largest overlap with the emission band of DCM, resulting in the largest fluorescence enhancement. In addition, the emission lifetime of C343 is shortest in the presence of SCF1 (1.82 ns), although the strongest fluorescence enhancement occurs with SCF6 (1.97 ns). These small discrepancies between the fluorescence enhancements and lifetime reductions may indicate the existence of contributions from fluorescence quenching or the excitation enhancements to the observed fluorescence enhancements of the dyes with the SCFs, in addition to the plasmon-coupled emission enhancements.

To analyze the relative contributions to the total fluorescence enhancements E_{tot} of dyes further, including the excitation enhancement E_{ex} caused by the strong local electric field, the emission enhancement E_{em} caused by the plasmon-coupled emission of metal nanoparticles, and the fluorescence quenching, the semi-empirical models based on emission kinetics measurements were recently introduced.[17,47,57] The radiative decay rate constant Γ_0 and non-radiative decay rate constant k_{nr} can be estimated from the fluorescence lifetime τ_0 and quantum yield Q_0 of a dye measured without metal nanoparticles.

$$Q_0 = \frac{\Gamma_0}{\Gamma_0 + k_{\text{nr}}} = \tau_0 \Gamma_0 \qquad (1)$$

The quantum yield of a dye in the presence of metal nanosurfaces Q_{m} is described similarly by the radiative decay rate constant Γ_{m} and the non-radiative decay rate constant $k_{\text{nr,m}}$ with metal nanosurfaces.

$$Q_{\text{m}} = \frac{\Gamma_{\text{m}}}{\Gamma_{\text{m}} + k_{\text{nr,m}}} = \tau_{\text{m}} \Gamma_{\text{m}} \qquad (2)$$

Γ_{m} and $k_{\text{nr,m}}$ include modified relaxation rates caused by plasmon-coupled emission and fluorescence quenching by metal nanosurfaces, respectively.[3,47,57] Thus, Γ_{m} and $k_{\text{nr,m}}$ are

determined from the fluorescence lifetime, τ_m and Q_m, which are determined from the emission enhancement E_{em} and Q_0.

$$E_{em} = Q_m/Q_0 = (\tau_m/\tau_0\Gamma_0)\Gamma_m \qquad (3)$$

To determine all of the radiative and non-radiative rate constants, the quantities of the excitation (E_{ex}) and emission enhancements (E_{em}) should be determined based on the total fluorescence enhancements E_{tot}.

$$E_{ex} = E_{tot}/E_{em} \qquad (4)$$

Xie *et al.* evaluated the E_{ex}, E_{em}, and Γ_m values of epi-cocconone dye with gold colloidal nanofilms based on the assumption of $k_{nr} = k_{nr,m}$, where bovine serum albumin was used as a spacer (approximately 12 nm thick) between the dye and the nanoparticles to minimize fluorescence quenching.[47] However, the assumption of an unmodified k_{nr} may not be applicable to this study as partial quenching of the fluorescences of dyes coated in thin PS layers on the SCFs may be unavoidable.[17]

We recently proposed an improved semi-empirical model for the analysis of the MEF mechanism by combining emission kinetics measurements for fluorescence lifetimes and quantum yields of dyes and the FDTD simulation results for local electric fields around metal nanoparticles.[17] The total fluorescence enhancement E_{tot} of a dye in the presence of a specific metal nanosurface can be interpreted as being equal to the excitation enhancement E_{ex} when the spectral overlap between the dipole and quadrupole SPR bands of the metal nanosurface and dyes' emission bands is poor, and no apparent emission lifetime reductions are observed. From the ratio of E_{ex} obtained for the SCF with poor spectral overlap to the local electric field increase evaluated from the FDTD simulations, all of the E_{ex} values for the rest of SCFs, which shows more of less spectral overlap with the emission of a dye can be estimated from results of FDTD simulations. Then, the entire MEF mechanism including the E_{ex}, E_{em}, Γ_m, and $k_{nr,m}$ values of the dyes, which depend on the sizes of silver nanoparticles, can be understood. However, differentiation between E_{em} and E_{ex} using the improved semi-empirical model may not be possible in the fluorescence enhancements of DCM, DNBP, and C343 with SCFs since the fluorescence enhancement solely by the electric field effect is not implemented due to unavoidable spectral overlap with the dipole and quadrupole SPR bands of all of the SCFs used in this study. In other words, the dyes exhibit significant lifetime reductions in the presence of each SCF, as shown in Fig. 4. The lifetime reduction represents the contribution of the plasmon-coupled emission to fluorescence enhancement. Alternatively, only the relative values for E_{ex} and E_{em} can be estimated for these dyes in the presence of SCFs.

Fig. 5(a) shows the local electric field distributions around the silver nanoparticles of SCF1–SCF8 (59–219 nm in diameter), as determined from FDTD simulations. The squares of the electric field amplitudes within the 0–50 nm range from the surface of each silver nanoparticle are averaged, and the resulting $|E_{loc}/E_0|^2$ values are plotted as a function of the average
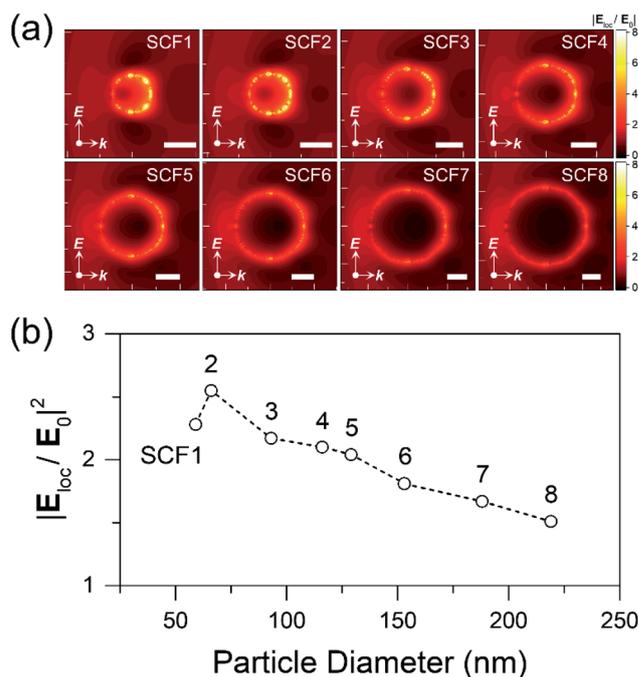

Fig. 5 (a) Local electric field distributions around the silver nanoparticles, SCF1–SCF8 of 59–219 nm in diameter, (b) $|E_{loc}/E_0|^2$ values averaged within 50 nm of the surface of each nanoparticle as a function of the average nanoparticle diameter. All of the scale bars in the FDTD simulation results are 50 nm long.

particle diameter in Fig. 5(b). The $|E_{loc}/E_0|^2$ of SCF2 (66 nm diameter) appears to be the largest and decreases gradually as the particle diameter increases towards 219 nm (SCF8). Using the proportionality coefficient γ between E_{ex} and $|E_{loc}/E_0|^2$,

$$E_{ex} = \gamma|E_{loc}/E_0|^2 \qquad (5)$$

the E_{em} values of a dye with SCFs can be evaluated from the E_{tot}.

$$E_{em} = \frac{E_{tot}}{\gamma|E_{loc}/E_0|^2} \qquad (6)$$

Then, the Γ_m and $k_{nr,m}$ of a dye with SCFs can be evaluated by combining eqn (2) and (3).

$$\Gamma_m = \frac{Q_0}{\tau_m} \times E_{em} \quad \text{and} \quad k_{nr,m} = \frac{1 - Q_0 \times E_{em}}{\tau_m} \qquad (7)$$

Although the exact value of the proportionality constant γ cannot be determined from the fluorescence enhancements of the dyes used in this study, the appropriate values can be estimated by referring to the resultant radiative (Γ_m) and non-radiative rate constants ($k_{nr,m}$). A γ value of 1.27 is suggested for the cases where the Γ_m and $k_{nr,m}$ values of DCM and DNBP in the presence of any SCF appear larger than the Γ_0 and k_{nr} values obtained without SCFs. In our previous report on the fluorescence enhancement of rhodamine 700 with SCFs, a similar value of $\gamma = 1.07$ was identified based on fluorescence measurements and local electric field simulations by the FDTD

method.[17] However, it seems that the proportionality constant γ = 1.27 may not be compatible with the fluorescence enhancements of all three dyes used in this work. Since the decrease in the emission lifetime of C343 was quite small with SCF4 (2.54 → 2.47 ns), the fluorescence enhancement with SCF4 can be attributed solely to excitation enhancement. The local field increase, $|E_{loc}/E_0|^2 = 2.10$ with SCF4, is approximately the same as total fluorescence enhancement of C343. Thus, the proportionality constant $\gamma = 1.00$ is used for C343.

Fig. 6 shows the E_{ex} and E_{em} values of dyes evaluated with the $\gamma = 1.27$ (for DCM and DNBP) and $\gamma = 1.00$ (for C343) as a function of the dipole SPR wavelength of SCFs. The variations in the Γ_m and $k_{nr,m}$ values of dyes with the SCFs by the choice of the proportionality coefficient γ are visualized in Fig. S6.† Table 2 summarizes detailed fluorescence enhancement results including the radiative and non-radiative rate constants of dyes
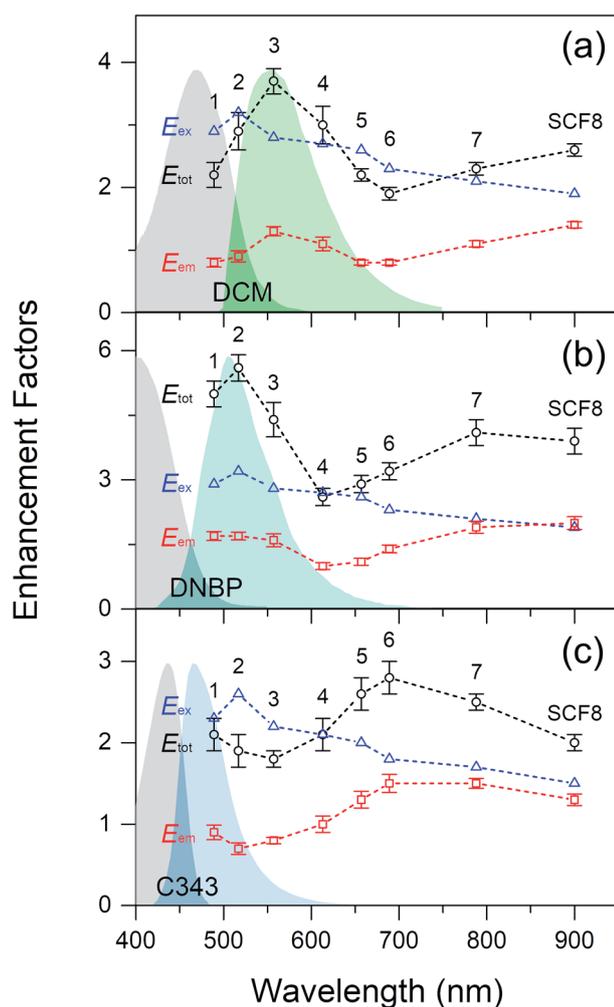
Table 2 Fluorescence enhancements and radiative and non-radiative rate constants of DCM, DNBP, and C343 with the SCFs[a]

SCF	τ_m (ns)	E_{tot}	$|E_{loc}/E_0|^2$	E_{ex}	E_{em}	Γ_m (10^8 s^{-1})	$k_{nr,m}$ (10^8 s^{-1})
DCM ($\tau_0 = 1.49$ ns, $Q_0 = 0.47^b$)							
SCF1	0.99	2.2	2.28	2.9	0.8	3.57	6.50
SCF2	0.88	2.9	2.55	3.2	0.9	4.73	6.59
SCF3	1.03	3.7	2.17	2.8	1.3	6.08	3.62
SCF4	1.19	3.0	2.10	2.7	1.1	4.41	3.99
SCF5	1.26	2.2	2.04	2.6	0.8	3.14	4.79
SCF6	1.20	1.9	1.81	2.3	0.8	3.23	5.14
SCF7	1.04	2.3	1.67	2.1	1.1	4.86	4.73
SCF8	0.93	2.6	1.51	1.9	1.4	6.80	3.94
DNBP ($\tau_0 = 2.12$ ns, $Q_0 = 0.13^b$)							
SCF1	1.21	5.0	2.28	2.9	1.7	1.90	6.33
SCF2	1.23	5.6	2.55	3.2	1.7	1.89	6.27
SCF3	1.40	4.4	2.17	2.8	1.6	1.53	5.60
SCF4	1.88	2.6	2.10	2.7	1.0	0.70	4.64
SCF5	1.73	2.9	2.04	2.6	1.1	0.87	4.90
SCF6	1.64	3.2	1.81	2.3	1.4	1.14	4.97
SCF7	1.33	4.1	1.67	2.1	1.9	1.95	5.57
SCF8	1.41	3.9	1.51	1.9	2.0	1.93	5.16
C343 ($\tau_0 = 2.54$ ns, $Q_0 = 0.59^b$)							
SCF1	1.82	2.1	2.28	2.3	0.9	3.01	2.49
SCF2	2.05	1.9	2.55	2.6	0.7	2.15	2.71
SCF3	2.34	1.8	2.17	2.2	0.8	2.10	2.16
SCF4	2.47	2.1	2.10	2.1	1.0	2.41	1.65
SCF5	2.20	2.6	2.04	2.0	1.3	3.44	1.10
SCF6	1.97	2.8	1.81	1.8	1.5	4.67	0.41
SCF7	2.19	2.5	1.67	1.7	1.5	4.05	0.50
SCF8	2.27	2.0	1.51	1.5	1.3	3.47	0.94

[a] τ_0: average lifetimes of dyes without the SCFs; Q_0: quantum yields of dyes without the SCFs; τ_m: average lifetimes with SCFs; E_{tot}: corrected total fluorescence enhancement factors; $|E_{loc}/E_0|^2$: averaged electric field strength within 50 nm of each silver nanoparticle surface, as calculated *via* FDTD simulations; E_{em}: emission enhancement factors; E_{ex}: excitation enhancement factors; Γ_m: radiative decay rates with SCFs; $k_{nr,m}$: non-radiative decay rates with the SCFs; the proportionality constants $\gamma = 1.27$ for DCM and DNBP, and $\gamma = 1.00$ for C343 were used. [b] Q_0 values of dyes in thin PS layers are evaluated by referring to that of DCM in a thin PS film.[17]

Fig. 6 The relative emission enhancement (E_{em}) of each dye is evaluated as the ratio of the total enhancement (E_{tot}) to the relative excitation enhancement (E_{ex}) from the local electric field simulations. The excitation enhancements with SCFs are estimated using the proportionality constants: $\gamma = 1.27$ for DCM and DNBP, and $\gamma = 1.00$ for C343. The absorption and emission spectra of each dye are also displayed for comparison.

with SCFs. As shown in Fig. 6, the dependence of E_{em} values of the three dyes on silver nanoparticle size appears quite similar to those of the total fluorescence enhancements, E_{tot}. As nanoparticle size increases, E_{ex} values only show small monotonous decrease. Thus, the E_{em} values appear to be heavily dependent on spectral overlap between the dyes' emission spectra and the dipole or quadrupole SPR bands of the SCFs. The dipole SPR of SCF3 (DCM) and SCF1 (DNBP), and the quadrupole SPR of SCF8 (DCM), SCF8 (DNBP), and SCF6 (C343) appear to maximize the E_{em} values. Given the large increases in the E_{em} values, the strong SCF-driven fluorescence enhancement of these dyes is attributed mainly to plasmon-coupled emission, which relies strongly on spectral overlap between the dyes' emission spectra and the dipole and quadrupole SPR bands.

It is interesting to note that the E_{em} values of DCM and DNBP under the influence of the quadrupole SPR of SCFs are 10–20% larger than those produced by dipole SPR. Despite the smaller

contribution to the electric field enhancements than the SCFs composed of smaller nanoparticles, the quadrupole SPR modes of SCFs composed of large nanoparticles result in substantial fluorescence enhancements for the three dyes. The fluorescence enhancement of C343 is largest with the quadrupole SPR mode of SCF6, where the dipole SPR-induced emission enhancement is not observed due to small spectral overlap between the emission and the SPR mode of the smallest SCF, which is SCF1. This shows clearly that plasmon-coupled emission dominates the SCF-driven fluorescence enhancement of the three dyes when substantial spectral overlap exists between the dipole or quadrupole SPR modes and the emission spectrum.

The Γ_m values of DCM and DNBP exhibit large SCF-driven increases when the spectral overlap between the dyes' emission and the dipole or quadrupole SPR bands of SCFs is large. The Γ_m values of DCM and DNBP in the presence of SCFs with strong quadrupole SPR bands (SCF8 and SCF7, respectively) appear similar to or slightly larger than those generated in the presence of SCFs with strong dipole bands (SCF3 and SCF1–2, respectively). This result is quite similar to the trend of E_{em} in the presence of SCFs. The Γ_m values for C343 exhibit large increases of approximately two times with SCF6, where the quadrupole SPR bands are in good spectral overlap with the emission band of C343. The $k_{nr,m}$ values of DCM and DNBP increase substantially with SCF1 and SCF2, which may indicate unavoidable emission quenching with SCFs. SCFs composed of small nanoparticles (SCF1–2 with average diameters of 59–66 nm) represent larger absorption cross-sections than scattering in the shorter wavelengths of the dipole SPR bands,[58] which often results in increased emission quenching.[3,47,57] The $k_{nr,m}$ values of C343 are estimated to decrease substantially when SCFs that consist of large silver nanoparticles (SCF5–SCF8) are used. However, the reason for the decrease in $k_{nr,m}$ with the quadrupole SCFs is not clearly understood.

In general, SCFs that contain large nanoparticles exhibit well-developed quadrupole SPR bands on the short-wavelength side of the much broader dipole SPR bands. The large scattering portion of extinction spectra of the large nanoparticles aids in fluorescence enhancements of numerous chromophores whose emission bands spectrally overlap the quadrupole SPR bands in the blue-green region of the visible wavelengths or the dipole SPR bands in the near-infrared (700–900 nm) region.[3,13,16,58] However, emission quenching of fluorophores by the absorption portion of the extinction spectra of SCFs may be difficult to reveal since the absorption and scattering portions of the dipole and quadrupole SPR bands may overlap each other spectrally. As shown in Fig. 2(a), the quadrupole SPR bands of SCF6–SCF8 exhibit good spectral overlap with the dipole SPR bands of SCF1–SCF3 in the blue-green wavelengths. Since the quadrupole SPR bands of large nanoparticles exhibit more scattering portion of the extinction spectrum than the dipole SPR bands,[58] the quadrupole SPR bands of SCFs can be applied further to plasmon-coupled emission, which includes much less emission quenching.[3,13]

Ginger and co-workers reported the emission enhancements of CdSe quantum dots (QDs) by silver nanoprisms.[16] The largest emission enhancements and lifetime reductions of CdSe QDs

(quantum yields: 0.028–0.10) were observed when strong spectral overlap occurred between the QDs' emission and the dipole SPR bands of the silver nanoprisms. Similarly, van Hulst and co-workers reported emission enhancement of light-harvesting complex 2 (LH2; quantum yield = 0.10) by gold nanorods.[59] Strong emission enhancements and LH2 lifetime reductions were observed when the spectral overlap with the dipole SPR bands of the gold nanorods was 160 nm long. In particular, increases in the radiative and non-radiative rate constants by the nanorods were estimated from time-resolved fluorescence measurements and FDTD simulations. The radiative rate enhancements (Γ_m/Γ_0; Purcell factor) or the quantum yields with the metal nanorods (Q_m) are required for accurate evaluation of the radiative and non-radiative rate constants of LH2 with gold nanorods.

Using homogeneous silver colloidal nanoparticles with a wide diameter range (59–219 nm) enabled quantitative investigation of the emission enhancements of several dyes via time-resolved fluorescence measurements and electric field simulations of the volumes near the silver nanoparticles. Nonetheless, separation of excitation and emission enhancements requires an exact proportionality coefficient γ that can relate the excitation enhancement to the local field increases from the FDTD simulations. Due to the spectral overlap between the dyes' emission spectra and both the dipole and quadrupole SPR bands of the SCFs, the excitation enhancement portions of the dyes' fluorescence enhancements are not obtained in this work. Thus, the E_{ex} and E_{em} values for all SCFs are relative measures rather than accurate measures of fluorescence enhancements of the dyes via resonant excitation and plasmon-coupled emission of the dipole and quadrupole SPR bands of SCFs.

Fig. 7 shows the local electric field enhancements, $|E_{loc}/E_0|^2$ of the SCFs as determined using the FDTD method at the maximum emission wavelength for each chromophore (555 nm for DCM, 505 nm for DNBP, and 465 nm for C343), which is also compared to the fluorescence lifetime changes with SCFs. Overall, the electric field enhancements of the SCFs, which are estimated at the dyes' maximum emission wavelengths, appear consistent with the fluorescence lifetime changes of the dyes in the presence of the SCFs. The largest electric field enhancements due to the dipole SPR bands are expected from SCF2, SCF1, and SCF1 for metal-enhanced emission from DCM, DNBP, and C343, respectively. Interestingly, the electric field enhancements obtained at the emission maximum wavelengths of the three dyes appear proportional to the decreases in the fluorescence lifetimes in terms of the dipole SPR wavelength, as shown in Fig. 7(b). Electric field enhancements by the quadrupole SPR modes are largest when SCF6–SCF8, SCF5–SCF7, and SCF6 are used at the emission maxima of DCM, DNBP, and C343, respectively. The largest emission lifetime changes are observed with SCF8 (DCM), SCF7 (DNBP), and SCF6 (C343). It seems that the electric field enhancements from the FDTD simulations at the emission maximum wavelengths of the dyes are good estimates of the fluorescence enhancements of dyes due to the dipole and quadrupole SPR of SCFs. This was reported previously for fluorescence enhancement of crystal violet with the SPR of gold nanorods, which depends heavily on the
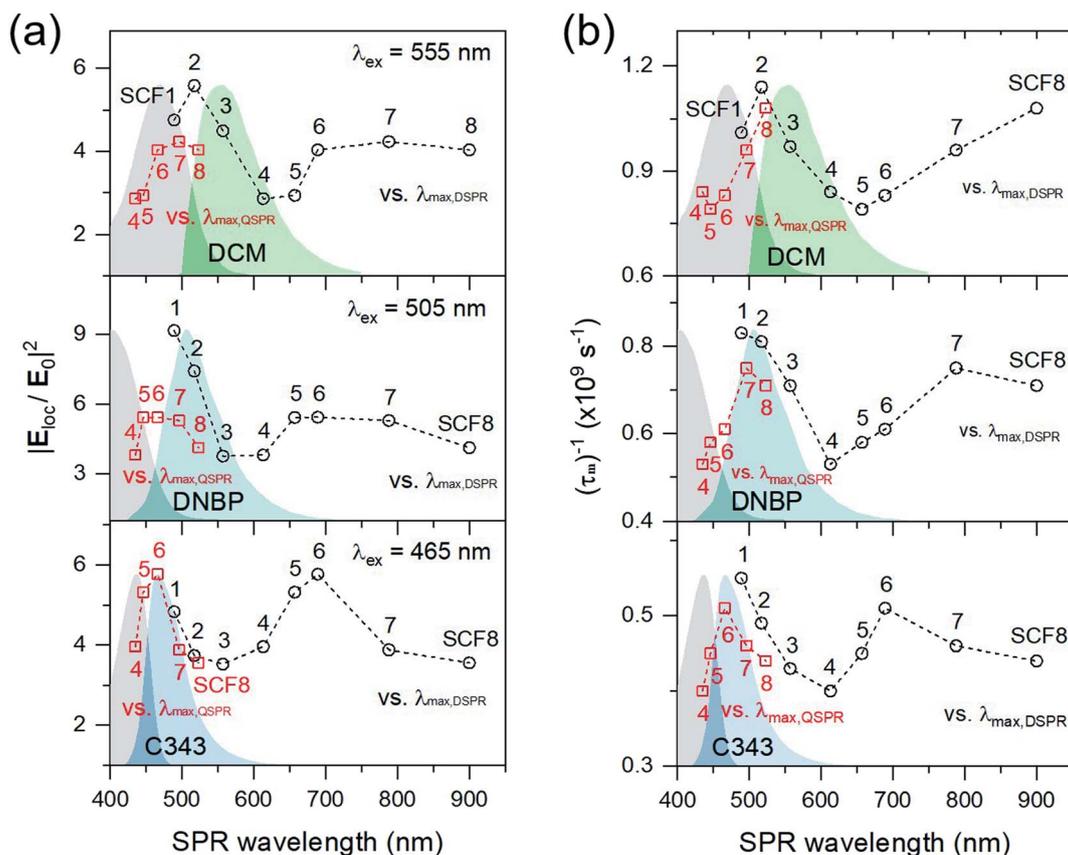
Fig. 7 (a) Local electric field enhancements ($|E_{loc}/E_0|^2$) of SCFs based on FDTD simulations performed at the emission maximum (λ_{em}) of each dye; the average within 50 nm of the surface of each nanoparticle is displayed as a function of the dipole ($\lambda_{max,DSPR}$) and quadrupole SPR wavelengths ($\lambda_{max,QSPR}$). (b) The inverse of the fluorescence lifetimes (τ_m^{-1}) of each dye displayed as a function of the dipole ($\lambda_{max,DSPR}$) and quadrupole SPR wavelengths ($\lambda_{max,QSPR}$). The absorption and emission spectra of each dye are also compared to the local electric field enhancements and fluorescence lifetime decreases with the SCFs.

aspect ratio of nanorods.[11] Nonetheless, the estimated electric field enhancements by FDTD simulations are slightly different from the emission lifetime changes that arise from plasmon-coupled emission of dyes. Fluorescence quenching that occurs *via* Förster type resonance energy transfers depends on the distance and the spectral overlap between the dyes and metal nanoparticles, and may lead to minor differences between the experimental fluorescence enhancements (or emission lifetime changes) and the electric field enhancements at the excitation and emission wavelengths of the fluorescence measurements.[60] Further experimental modifications are required to minimize non-radiative quenching of dyes' emissions that originate from direct contact with metal nanoparticles, which will be addressed in future works.

In this work, we have investigated emission enhancement of three dyes, DCM, DNBP, and C343, by SCFs with dipole and quadrupole SPR bands that span a wide range of visible to near-infrared wavelengths. Furthermore, emission enhancement by nanoparticles with quadrupole SPR bands has been reported previously, where the emission enhancements due to the in-plane quadrupole resonance of large silver nanoplates have been suggested to be more efficient than the enhancements *via* dipole resonance of small nanoplates.[38] In this report, we compare the

fluorescence enhancements of chromophores between the dipole and quadrupole SPR bands of SCFs *via* combined investigation of time-resolved fluorescence measurements and FDTD simulations of local electric field distributions. Chromophore's fluorescence is enhanced substantially by increases in the local electric field and plasmon-coupled emission *via* the SPR bands of metal nanoparticles. Moreover, we are the first to report that plasmon-coupled emissions *via* both the dipole and quadrupole SPR modes of the SCFs depend strongly on spectral overlap with the chromophores' emission bands. SCFs composed of homogeneous silver nanoparticles with well-developed SPR bands in the blue-green wavelengths can be useful in numerous applications, including photonics, bioimaging, and chemical sensors. For example, we recently reported that composite SCFs synthesized from small and large nanoparticles produce optimized fluorescence enhancement with a specific dye molecule, especially when the dipole SPR bands of the small nanoparticles and the quadrupole SPR bands of the large nanoparticles provide good spectral overlap with the emission spectrum of the dye.[61]

Conclusions

SCFs made from silver nanoparticles 59–219 nm in diameter were synthesized *via* kinetically controlled seeded-growth, and

used to enhance the fluorescence of DCM, DNBP, and C343. The SCFs exhibit dipole and quadrupole SPR bands at a wide range of wavelengths that depend on the particle size, which are clearly distinguished from each other *via* the well-dispersed silver nanoparticles on the substrates. The fluorescence of dyes spin-coated in thin PS layers increased substantially, and large emission lifetime decreases were observed when the dyes' emission bands overlap with the dipole SPR bands of SCFs composed of small silver nanoparticles. Strong fluorescence enhancements and lifetime reductions of dyes were also observed, as the emission bands of dyes overlap greatly with the quadrupole SPR bands of SCFs composed of large silver nanoparticles. Interestingly, while DCM and DNBP exhibited the strongest fluorescence enhancements with the dipole SPR of SCFs, the fluorescence of C343 was enhanced most by the quadrupole SPR of SCFs. Using the estimated relative enhancement factors and relaxation rates of dyes in the presence of each SCF, an improved semi-empirical model was used to interpret the fluorescence enhancements of dyes as being attributed mainly to the plasmon-coupled emission that accompanies energy transfer between the excited dyes and the dipole or quadrupole SPR modes of the SCFs. Furthermore, the stronger fluorescence enhancement of C343 with the quadrupole SPR of SCFs was explained as larger radiative decay rates and smaller non-radiative decay rates by the scattering portion of the quadrupole SPR bands of large silver nanoparticles than those by the absorption of the dipole SPR bands of small nanoparticles. We expect that the quadrupole SPR modes of the SCFs can be used as frequently as the dipole SPR modes to achieve efficient fluorescence enhancement of various dyes.

Author contributions

Daedu Lee: investigation, formal analysis, writing – original draft. Junghyun Song: investigation. Gyounghyun Song: investigation. Yoonsoo Pang: conceptualization, supervision, writing – review & editing.

Conflicts of interest

There are no conflicts to declare.

Acknowledgements

References

1 J. R. Lakowicz, K. Ray, M. Chowdhury, H. Szmacinski, Y. Fu, J. Zhang and K. Nowaczyk, *Analyst*, 2008, **133**, 1308–1346.
2 S. M. Fothergill, C. Joyce and F. Xie, *Nanoscale*, 2018, **10**, 20914–20929.
3 J. R. Lakowicz, *Anal. Biochem.*, 2005, **337**, 171–194.
4 M. Pelton, *Nat. Photonics*, 2015, **9**, 427.
5 P. A. Hobson, S. Wedge, J. A. E. Wasey, I. Sage and W. L. Barnes, *Adv. Mater.*, 2002, **14**, 1393–1396.
6 Y. Jeong, Y.-M. Kook, K. Lee and W.-G. Koh, *Biosens. Bioelectron.*, 2018, **111**, 102–116.
7 Y. Pang, Z. Rong, R. Xiao and S. Wang, *Sci. Rep.*, 2015, **5**, 9451.
8 C. D. Geddes and J. R. Lakowicz, *J. Fluoresc.*, 2002, **12**, 121–129.
9 T. Ming, H. Chen, R. Jiang, Q. Li and J. Wang, *J. Phys. Chem. Lett.*, 2012, **3**, 191–202.
10 Y. Chen, K. Munechika, I. Jen-La Plante, A. M. Munro, S. E. Skrabalak, Y. Xia and D. S. Ginger, *Appl. Phys. Lett.*, 2008, **93**, 053106.
11 S. Khatua, P. M. R. Paulo, H. Yuan, A. Gupta, P. Zijlstra and M. Orrit, *ACS Nano*, 2014, **8**, 4440–4449.
12 H. Y. Liang, H. G. Zhao, Z. P. Li, C. Harnagea and D. L. Ma, *Nanoscale*, 2016, **8**, 4882–4887.
13 Y. Zhang, A. Dragan and C. D. Geddes, *J. Phys. Chem. C*, 2009, **113**, 12095–12100.
14 F. Tam, G. P. Goodrich, B. R. Johnson and N. J. Halas, *Nano Lett.*, 2007, **7**, 496–501.
15 Y. Chen, K. Munechika and D. S. Ginger, *Nano Lett.*, 2007, **7**, 690–696.
16 K. Munechika, Y. Chen, A. F. Tillack, A. P. Kulkarni, I. J. L. Plante, A. M. Munro and D. S. Ginger, *Nano Lett.*, 2010, **10**, 2598–2603.
17 D. Lee, J. Lee, J. Song, M. Jen and Y. Pang, *Phys. Chem. Chem. Phys.*, 2019, **21**, 11599–11607.
18 J. Lee, S. Lee, M. Jen and Y. Pang, *J. Phys. Chem. C*, 2015, **119**, 23285–23291.
19 J. Lee, J. Song, D. Lee and Y. Pang, *Sci. Rep.*, 2019, **9**, 3551.
20 M. Li, S. K. Cushing and N. Wu, *Analyst*, 2015, **140**, 386–406.
21 P. Anger, P. Bharadwaj and L. Novotny, *Phys. Rev. Lett.*, 2006, **96**, 113002.
22 K. Ray, H. Szmacinski, J. Enderlein and J. R. Lakowicz, *Appl. Phys. Lett.*, 2007, **90**, 251116.
23 T. Ming, L. Zhao, H. Chen, K. C. Woo, J. Wang and H.-Q. Lin, *Nano Lett.*, 2011, **11**, 2296–2303.
24 N. Liu, B. S. Prall and V. I. Klimov, *J. Am. Chem. Soc.*, 2006, **128**, 15362–15363.
25 P. Viste, J. Plain, R. Jaffiol, A. Vial, P. M. Adam and P. Royer, *ACS Nano*, 2010, **4**, 759–764.
26 P. Reineck, D. Gómez, S. H. Ng, M. Karg, T. Bell, P. Mulvaney and U. Bach, *ACS Nano*, 2013, **7**, 6636–6648.
27 A. L. Feng, M. L. You, L. Tian, S. Singamaneni, M. Liu, Z. Duan, T. J. Lu, F. Xu and M. Lin, *Sci. Rep.*, 2015, **5**, 7779.
28 C. Chen, L. Zhang, M. Yang, C. Tao, Z. Han, B. Chen and H. Zeng, *Opt. Express*, 2017, **25**, 9901–9910.
29 D. Cheng and Q.-H. Xu, *Chem. Commun.*, 2007, 248–250, DOI: **10.1039/B612401A**.
30 S. Li, T. Zhang, Z. Zhu, N. Gao and Q.-H. Xu, *RSC Adv.*, 2016, **6**, 58566–58572.
31 K. L. Kelly, E. Coronado, L. L. Zhao and G. C. Schatz, *J. Phys. Chem. B*, 2003, **107**, 668–677.
32 B. Bhushan, *Encyclopedia of Nanotechnology*, Springer Netherlands, Dordrecht, 2016.

33 G. V. Hartland, *Chem. Rev.*, 2011, **111**, 3858–3887.

34 N. G. Bastús, J. Piella and V. Puntes, *Langmuir*, 2016, **32**, 290–300.

35 M. Rycenga, C. M. Cobley, J. Zeng, W. Li, C. H. Moran, Q. Zhang, D. Qin and Y. Xia, *Chem. Rev.*, 2011, **111**, 3669–3712.

36 F. Zhou, Z.-Y. Li, Y. Liu and Y. Xia, *J. Phys. Chem. C*, 2008, **112**, 20233–20240.

37 Q. Zhang, W. Li, C. Moran, J. Zeng, J. Chen, L.-P. Wen and Y. Xia, *J. Am. Chem. Soc.*, 2010, **132**, 11372–11378.

38 Y. Shen, T. He, W. Wang, Y. Zhan, X. Hu, B. Yuan and X. Zhou, *Nanoscale*, 2015, **7**, 20132–20141.

39 B. J. Wiley, S. H. Im, Z.-Y. Li, J. McLellan, A. Siekkinen and Y. Xia, *J. Phys. Chem. B*, 2006, **110**, 15666–15675.

40 N. G. Bastús, F. Merkoçi, J. Piella and V. Puntes, *Chem. Mater.*, 2014, **26**, 2836–2846.

41 N. G. Bastús, J. Comenge and V. Puntes, *Langmuir*, 2011, **27**, 11098–11105.

42 M. Chakraborty, D. Chowdhury and A. Chattopadhyay, *J. Chem. Educ.*, 2003, **80**, 806.

43 P. D. T. Huibers and D. O. Shah, *Langmuir*, 1997, **13**, 5995–5998.

44 S. Lee, J. Lee and Y. Pang, *Curr. Appl. Phys.*, 2015, **15**, 1492–1499.

45 E. D. Palik, *Handbook of Optical Constants of Solids*, Academic Press, Boston, 1985.

46 J. Kim, G. Dantelle, A. Revaux, M. Bérard, A. Huignard, T. Gacoin and J.-P. Boilot, *Langmuir*, 2010, **26**, 8842–8849.

47 F. Xie, M. S. Baker and E. M. Goldys, *Chem. Mater.*, 2008, **20**, 1788–1797.

48 T. Nakamura and S. Hayashi, *Jpn. J. Appl. Phys.*, 2005, **44**, 6833.

49 H. Dai, J. Zhao, T. Huang, X. Yu, J. Sun, H. Fang, Z. Zhu, M. Zhang and K. Yu, *Appl. Sci.*, 2018, **8**, 897.

50 W.-S. Chae, J. Yun, S.-H. Nam, S.-G. Lee, W.-G. Yang, H. Yoon, M. Park and S. Jeon, *ACS Appl. Mater. Interfaces*, 2018, **10**, 14079–14086.

51 J. Zhu, L. Sun, Y. Shan, Y. Zhi, J. Chen, B. Dou and W. Su, *Vacuum*, 2021, **187**, 110096.

52 J. Hao, M.-J. Han, Z. Xu, J. Li and X. Meng, *Nanoscale Res. Lett.*, 2011, **6**, 263.

53 G. Chumanov, K. Sokolov, B. W. Gregory and T. M. Cotton, *J. Phys. Chem.*, 1995, **99**, 9466–9471.

54 G. Kwak, C. Okada, M. Fujiki, H. Takeda, T. Nishida and T. Shiosaki, *Jpn. J. Appl. Phys.*, 2008, **47**, 1753–1756.

55 G. M. Akselrod, M. C. Weidman, Y. Li, C. Argyropoulos, W. A. Tisdale and M. H. Mikkelsen, *ACS Photonics*, 2016, **3**, 1741–1746.

56 O. Kedem, W. Wohlleben and I. Rubinstein, *Nanoscale*, 2014, **6**, 15134–15143.

57 I. G. Theodorou, Z. A. R. Jawad, Q. Jiang, E. O. Aboagye, A. E. Porter, M. P. Ryan and F. Xie, *Chem. Mater.*, 2017, **29**, 6916–6926.

58 D. D. Evanoff and G. Chumanov, *J. Phys. Chem. B*, 2004, **108**, 13957–13962.

59 E. Wientjes, J. Renger, A. G. Curto, R. Cogdell and N. F. van Hulst, *Phys. Chem. Chem. Phys.*, 2014, **16**, 24739–24746.

60 T. Ming, L. Zhao, Z. Yang, H. Chen, L. Sun, J. Wang and C. Yan, *Nano Lett.*, 2009, **9**, 3896–3903.

61 D. Lee, G. Song and Y. Pang, *Bull. Korean Chem. Soc.*, 2022, **43**, 35–39.